

Redox mechanism in the binary transition metal phosphide Cu_3P

B. Mauvernay^a, M.-L. Doublet^b, L. Monconduit^{a,*}

^a LAMMI—CNRS 5072, Université Montpellier II, Place Eugène Bataillon, 34095 Montpellier Cedex 5, France

^b LSDSMS—CNRS 5636, Université Montpellier II, Place Eugène Bataillon, 34095 Montpellier Cedex 5, France

Abstract

The electrochemical behaviour of the binary transition metal phosphide Cu_3P towards lithium is investigated through galvanic and potentiostatic measurements. Obtained through high-temperature synthesis, this system shows a better volumetric capacity than graphite and a good capacity retention. In situ X-ray diffraction and first-principles electronic structure calculations are combined with the electrochemical results to show that the complete insertion of 3Li^+ in the Cu_3P electrode proceeds with the formation of three intermediate phases of lithium composition $\text{Li}_x\text{Cu}_{(3-x)}\text{P}$ ($x=1,2,3$). The extra capacity previously observed in discharge is now clearly assigned to lithium insertion into the CuP_2 impurity and to SEI reactions.

© 2006 Elsevier Ltd. All rights reserved.

1. Introduction

The search for electrode materials alternative to graphitic carbon in rechargeable lithium-ion batteries is a major topic in the area of energy storage, and interests in study of new families of negative electrode materials for secondary batteries. In this field, transition metal phosphides (TM-Phosphides) show very attractive performances, exhibiting large volumetric and specific capacities [1–4]. They are characterized by facile structural rearrangements that are correlated to easy lithium insertion and sometimes to reversible crystalline–amorphous transition, thanks to the strong covalent character of the M–P bonds. To meet the remarkable structural and electrochemical properties of ternary TM-Phosphides with the industrial requirements of using non-lithiated anodes, Cu_3P was recently proposed as a possible negative electrode material [5–8]. Different synthetic routes were investigated for that system in order to correlate its redox properties to the powder size and morphology [7]. Nano-structured materials were shown to favour high initial capacities, while micro-structured materials have led to better capacity retention than nano-structured and bulk materials. Powders obtained by solvothermal (ST) synthetic routes were shown to react with 5Li^+ instead of the 3Li^+ expected for a complete reaction $\text{Cu}_3\text{P} + 3\text{Li} \rightarrow \text{Li}_3\text{P} + 3\text{Cu}^0$. This suggests that extra reactions involving either the electrolyte or amorphous impurities can take place in these

ST-electrodes. High-temperature (HT) syntheses have thus been investigated to obtain well-crystallized samples, allowing in situ X-ray diffraction (XRD) analyses. First-principle electronic structure calculations including full structural relaxations have also been performed to follow the structural changes upon lithiation. Experimental and computational details are given Section 2. Galvanostatic and potentiodynamic measurements and in situ X-ray diffraction results are presented Section 3. Section 4 is devoted to the electrochemical mechanism upon cycling.

2. Experimental and computational details

Cu_3P was synthesized at high temperature with 2.8/1 ratio of copper metal and red phosphorus as powders in a sealed silica tube. The temperature was increased to 600 °C and held for 48 h. Cu_3P powder purity and crystallinity were studied by powder XRD which were recorded on a Philips X-pert diffractometer ($\text{Cu K}\alpha_1$).

Electrochemical lithium insertion/extraction experiments were performed in Swagelok™-type cells assembled in an argon-filled dry box. These cells consist of a composite electrode containing 10–12 mg of active material mixed with 15 wt% of acetylene black as positive electrode, a lithium metal disk as negative electrode, and a Whatman GF/D borosilicate glass microfiber separator saturated with 1 M LiPF_6 (EC:DMC, 1:1) electrolyte solution placed in between. Electrochemical insertion was monitored using a Mac Pile (Biologic SA) in the range 2.00–3.00 to 0.01 V. Various C/n scan rates were used, C/n representing for a full charge or discharge in n hours.

* Corresponding author.

E-mail address: moncondu@univ-montp2.fr (L. Monconduit).

In situ XRD were recorded using a D8 X-ray monochromated diffractometer ($\text{Co K}\alpha_1$), at various states of charge and discharge of the $\text{Li}/\text{Cu}_3\text{P}$ system, in potentiodynamic mode at a rate of $C/35$ ($\text{Li}/10$ h) and using a specifically designed electrochemical cell. The electrode material was sampled underneath a beryllium window used as current collector.

Electronic structure calculations were performed using the density functional theory (DFT) code VASP [9]. Full structural relaxations were carried out for various lithium contents in order to evaluate their relative stability. Projector augmented wave pseudo-potentials (PAW) [10] were used for the basis set, as they are expected to give a better description of alkali metal atoms than ultra-soft pseudo-potentials (US-PP) [11].

3. Results

High-temperature synthesis leads to average particles-size varying from 10 to 100 μm according to SEM measurements. The XRD of $\text{Cu}_3\text{P-HT}$ powder is shown in Fig. 1. The diffraction peaks were indexed as a single phase according to the hexagonal low temperature Cu_3P phase ($a=6.951(1)$ Å, $c=7.143(1)$ Å, $P6_3cm$) [12]. Very good agreement is obtained with theory since relaxed unit cell parameters calculated for the Cu_3P structure agree within the above to 2% ($a=6.976$ Å, $c=7.232$ Å) (Table 1).

As presented in Fig. 2, the galvanostatic curve obtained from in situ XRD measurements shows the insertion of 3.5Li^+ per Cu_3P during the first reduction down to 0.01 V/Li and the uptake of 2.5Li^+ per cell during oxidation from 0.01 to 2 V/Li. It shows successive voltage plateaus and slopes, both in charge and discharge.

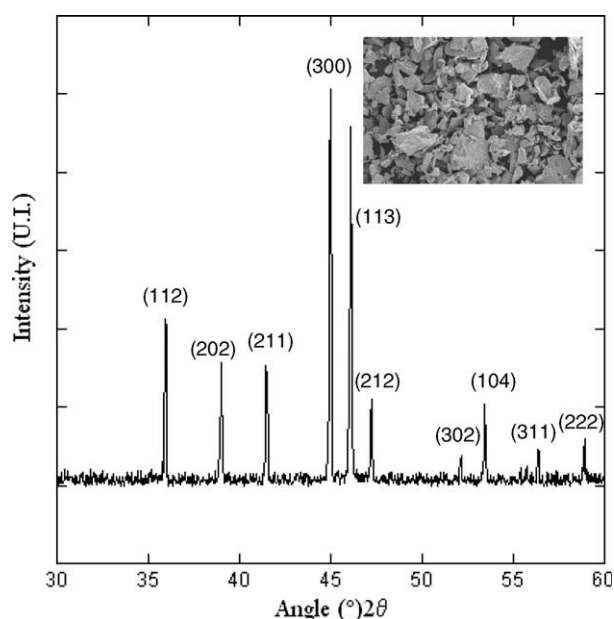


Fig. 1. X-ray diffraction patterns ($\text{Cu K}\alpha_1$) of Cu_3P prepared by ceramic route. Inset corresponds to the SEM image of Cu_3P powder as obtained.

Table 1
Unit cell parameters obtained for the relaxed Cu_3P , Li_2CuP , $\text{Li}_x\text{Cu}_{(3-x)}\text{P}$ ($x=1/3$ and 1) and Li_3P phases, compared to available experimental values (in parentheses)

System	$a=b$ (Å)	c (Å)	γ (°)
Cu_3P	6.976 (6.959)	7.232 (7.143)	120
$\text{Li}_{0.33}\text{Cu}_{2.66}\text{P}$ (1+2)	7.02	7.26	120.0
$\text{Li}_{0.33}\text{Cu}_{2.66}\text{P}$ (1+1)	7.06	7.25	121.2
$\text{Li}_{0.33}\text{Cu}_{2.66}\text{P}$ (2+2)	6.99	7.29	119.6
LiCu_2P	7.15	7.28	120.0
Li_2CuP	4.027 (4.045)	7.791 (7.724)	120.0
Li_3P	4.230 (4.264)	7.562 (7.579)	120.0

For $\text{Li}_{0.33}\text{Cu}_{2.66}\text{P}$, (1+2) (1+1) and (2+2) refer to three different Li/Cu substitutions of Cu(1) and/or Cu(2).

Potentiodynamic measurements were carried out for the two first discharges and charges using a low scan rate ($C/35$). The resulting curve presented in Fig. 3 clearly shows the complexity of the electrochemical processes, with six phenomena occurring during the first discharge (solid line): a shoulder at 0.95 V (S), three sharp peaks at 0.90 (1), 0.82 (2) and 0.65 V (I), and two broader complex peaks at ~ 0.18 (3) and ~ 0.02 V (4). Only five of these six peaks are observed in charge: two superimposed peaks at 0.71 (4') and 0.80 V (3'), and three distinct peaks at 1.06 (2'), 1.13 (1') and 1.29 V (0'). For the second discharge (dotted line), neither the shoulder (S), nor the incremental peak at 0.65 V (I) is observed. Hence, except for these two latter processes, a rather good electrochemical reversibility is observed.

The in situ XRD patterns collected are presented in Fig. 4a and b for the discharge, and Fig. 4c for the charge. Discharge corresponds to the reaction of 3.5Li^+ with the electrode (Fig. 2). Process (1) and its shoulder (S) correspond to the insertion of less than 0.5Li^+ in Cu_3P and were first associated

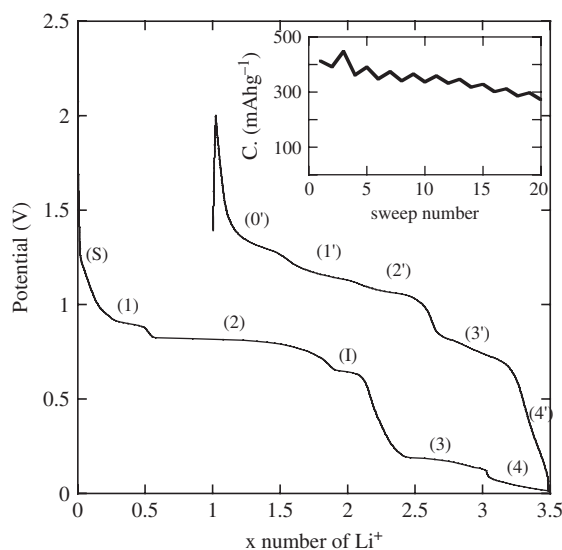


Fig. 2. Voltage–composition profile for $\text{Cu}_3\text{P}/\text{Li}$ cell used for the in situ X-ray collection data, at $C/35$ scan rate ($1\text{Li}/10$ h). The capacity retention for the 20 first cycles is shown in inset.

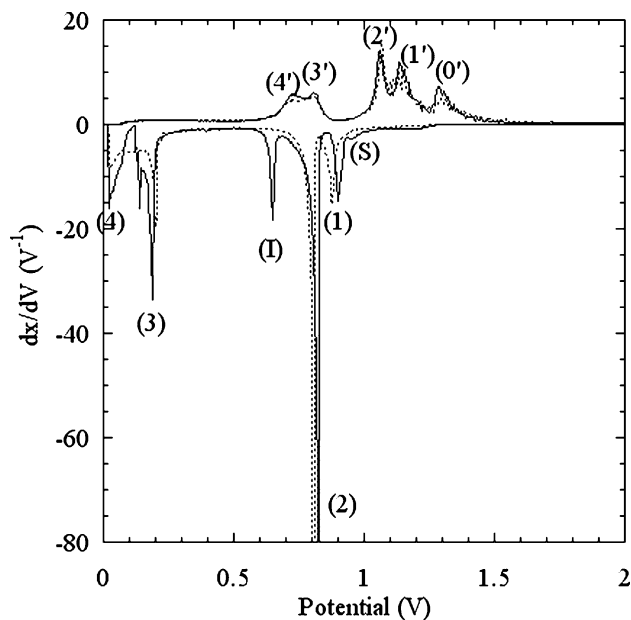


Fig. 3. Derivative dx/dV of the $\text{Cu}_3\text{P}/\text{Li}$ cell cycled for the first two cycles at a $C/35$ scan rate between 0 and 2 V (the second cycle appears in dotted line).

with a solid solution transformation: the characteristic Cu_3P diffraction peaks are shifted down to smaller angles as lithium is inserted, showing a slight increase of the pristine Cu_3P cell parameters (bottom of Fig. 4a). Surprisingly, after insertion of 0.2–0.3 (S) Li^+ , the electrode tends to show a better X-ray diffusing power than Cu_3P , as suggested by the relative increase of the (2 0 2) Cu_3P peak area plotted in Fig. 4d. This peak at 45.6° in 2θ shows suspicious oscillations. After a slight decrease, consistent with a classical solid solution mechanism, it reaches a maximum at $x \sim 0.2$ – 0.3 , and then drastically decreases down to $x = 0.5$. The maximum could be correlated to the formation of a new phase, exhibiting similar unit cell parameters and symmetry compared to Cu_3P . Nevertheless, as Cu_3P exhibits a very close-packed structure, the formation of a lithiated $\text{Li}_x\text{Cu}_3\text{P}$ phase, without any copper extrusion appears doubtful. More reliable hypotheses would be to consider a Li/Cu substitution occurs, at the very beginning of Li insertion, leading to finely divided Cu° particles not detected by XRD.

Process (2) corresponds to a significant insertion up to $x = 1.8$ and is associated with a two-phase transformation. As shown on the top of Fig. 4a, in situ XRD clearly shows that the decrease of the Cu_3P diffraction peaks comes with the growing of several new peaks ascribed to the Li_2CuP phase ($a = 4.045 \text{ \AA}$, $c = 7.724 \text{ \AA}$, $P\text{-}3m1$ (PCPDFD 25-0479)) and to the copper metal ((1 1 1) Cu° peak at 50.80° in 2θ). This reaction is clearly depicted Fig. 4d by a drastic increase of both the (1 1 1) Cu° peak area (black diamond) and the Li_2CuP peaks area (open triangles). Nevertheless, the Li_2CuP diffraction peaks keep on growing even when the Cu_3P diffraction peaks have completely disappeared. This suggests that an intermediate phase is probably formed, although not characterized by XRD. The third process (I) at $U = 0.65 \text{ V}$ and correlated to a sharp incremental peak in Fig. 3 leads to an insertion of $\sim 0.3 \text{ Li}^+$ and can be assigned to lithium insertion into the CuP_2 , an

impurity not detected by XRD. Actually, the first lithium insertion into CuP_2 (not shown here) is characterized by a flat voltage plateau at 0.65 V. As reported previously [4], and confirmed by the present study, this insertion process in CuP_2 is poorly reversible. The last two complex processes (3) and (4) between $U = 0.2$ and $U = 0.01 \text{ V}$ correspond to the insertion of about 1 Li^+ . For (3), the sharpness of this incremental peak suggests a two-phase process, while a single-phase process is expected for (4). In this potential range the Li_2CuP diffraction peaks drastically vanish (top of Fig. 4b) and the (1 1 1) Cu° peak slightly increases. It is thus tempting to assign (at least) one of these two processes to the reaction $\text{Li}_2\text{CuP} + \text{Li} \rightarrow \text{Li}_3\text{P} + \text{Cu}^\circ$. As shown in Fig. 4d, Cu° is not produced during process (3), suggesting that lithium reacts with either an impurity or the electrolyte. Li_3P should thus be formed during process (4) only, even though the concomitant electrode amorphization avoids any XRD proof for this hypothesis.

Charge. Upon charging, 2.5 Li^+ are extracted from the electrode (Fig. 2). The two processes (4') and (3') occur between 0.71 and 0.80 V, involving almost one Li^+ . Meanwhile, the in situ XRD patterns (Fig. 4c) show the formation of Li_2CuP . As for the discharge, Cu° is consumed only during (4') (Fig. 4e), showing that (4') and (3') correspond to the back reactions (4) and (3), respectively. The sharp peak at 1.06 V (2') corresponds to a drastic loss of the Li_2CuP diffraction peaks. The diffraction peaks of the Cu_3P phase (or the lithiated $\text{Li}_x\text{Cu}_{3-x}\text{P}$) are not observed during this process (Fig. 4e), supporting the fact that an intermediate X-ray amorphous phase is kinetically achieved in charge, delaying the formation of Cu_3P . This reaction could correspond to the formation of LiCu_2P , as already suggested in discharge. Such a hypothesis is strongly supported by the Cu° consumption observed during (2') in Fig. 4e, and by the occurrence of an extra peak at 53° which could be assigned to the main peak of the LiCu_2P structure (PCPDFD-25-0480). Process (1') at 1.13 V corresponds to a lithium extraction down to $x = 1.5$ (Fig. 2). It is associated with the consumption of Cu° as shown by in situ XRD (top of Fig. 4c and e). Note that the Cu_3P diffraction peaks are not seen, suggesting that an amorphous phase is formed. This phase is characterized by a greater Cu/Li ratio than in LiCu_2P but is undetectable by X-rays. Finally, the last process (0') is clearly assigned to the recovery of Cu_3P correlated with the complete consumption of Cu° . The lower capacity observed during the charge should obviously be related to the two irreversible processes occurring on discharge.

4. Discussion

Results presented above show that lithium insertion/extraction in $\text{Cu}_3\text{P-HT}$ occur through different pathways. For the first discharge, the complete reaction corresponds to the insertion of 3.5 Li^+ . Considering that the two irreversible processes characterized in discharge (namely S and I) involve about 0.5 lithium, a reversible reaction of about 3.0 lithium is therefore expected for this $\text{Cu}_3\text{P-HT}$ sample. This is fully consistent with the theoretical capacity expected for the complete reaction $\text{Cu}_3\text{P} + 3\text{Li} \leftrightarrow \text{Li}_3\text{P}$. As shown in Fig. 2 (inset), the voltage

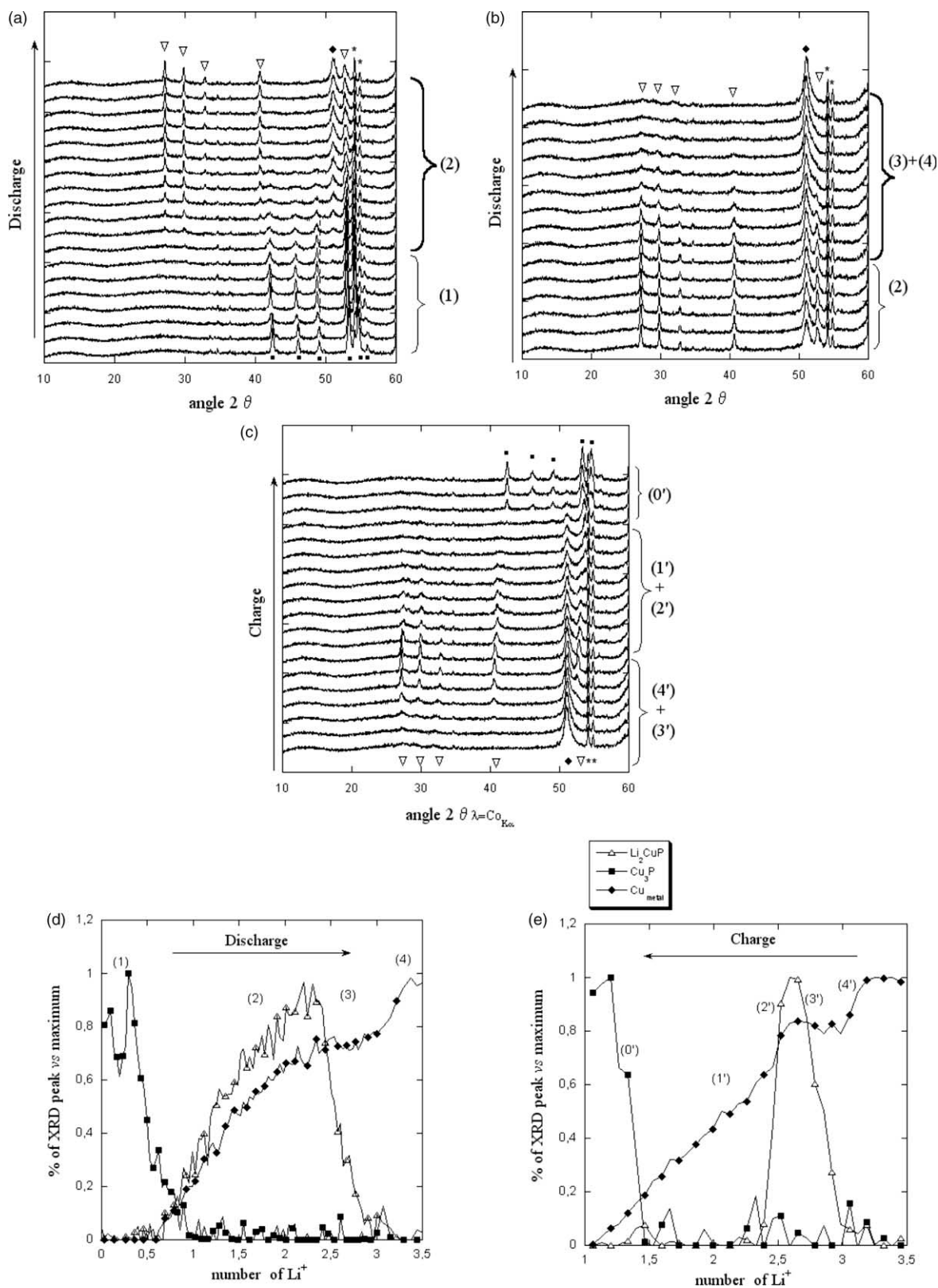
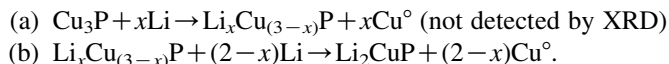


Fig. 4. In situ X-ray ($\text{Co K}\alpha_1$) diffraction patterns collected at various first cycle states of the $\text{Cu}_3\text{P}/\text{Li}$ electrochemical cell, (a) corresponding to the first part of the discharge, Cu_3P peaks shown by black squares (PCPDF-71-2261) and Be and BeO of the cell hardware by asterisk, (b) to the second part of the discharge. Li_2CuP peaks are identified by open triangles (PCPDF-25-0479), Cu metal by black square (PCPDF-04-0836). (c) Powder patterns corresponding to the first charge. On (d) the relative change of the diffraction peak area, calculated for the Cu_3P (2 0 2) peak located at 45.6° (black squares) the Li_2CuP (1 0 0) peak located at 26.8° (white triangles) and the Cu (1 1 1) peak located at 50.8° (black diamonds). These areas are plotted as a function of the inserted Li^+ number for the first discharge (d) and the first charge (e).

profile obtained shows a relatively good capacity retention for the first twenty sweeps of charge and discharge. It corresponds to a discharge capacity of 415 mAh/g (3193 mAh/cm³) out of which 390 mAh/g (3018 mAh/cm³) are reversible.

To elucidate the overall mechanism involved in the different reaction steps on discharge and charge, electronic structure calculations were performed and combined with the experimental results. Upon discharge, potentiodynamic measurements and in situ XRD have pointed to the formation of two intermediate phases, namely $\text{Li}_x\text{Cu}_{(3-x)}\text{P}$ ($0 < x < 0.5$) and Li_2CuP , respectively. These first two steps have been correlated to the extrusion of two moles of copper and would correspond to the two following reactions:



The Cu_3P crystal structure described in the $P6_3cm$ space group is presented in Fig. 5a. In this structure, four independent Cu atoms are found, namely Cu(1), Cu(2), Cu(3) and Cu(4). Cu(1) and Cu(2) lie in six-fold positions, while Cu(3) and Cu(4) are located in four- and two-fold positions, respectively. When lithium is inserted into the Cu_3P unit cell, our structural relaxations systematically lead to unstable phases, irrespective of the position chosen for the additional lithium atoms. This tends to question the mechanism proposed in Ref. [8] at the very beginning of the discharge, i.e. a monophasic lithium insertion in Cu_3P ,

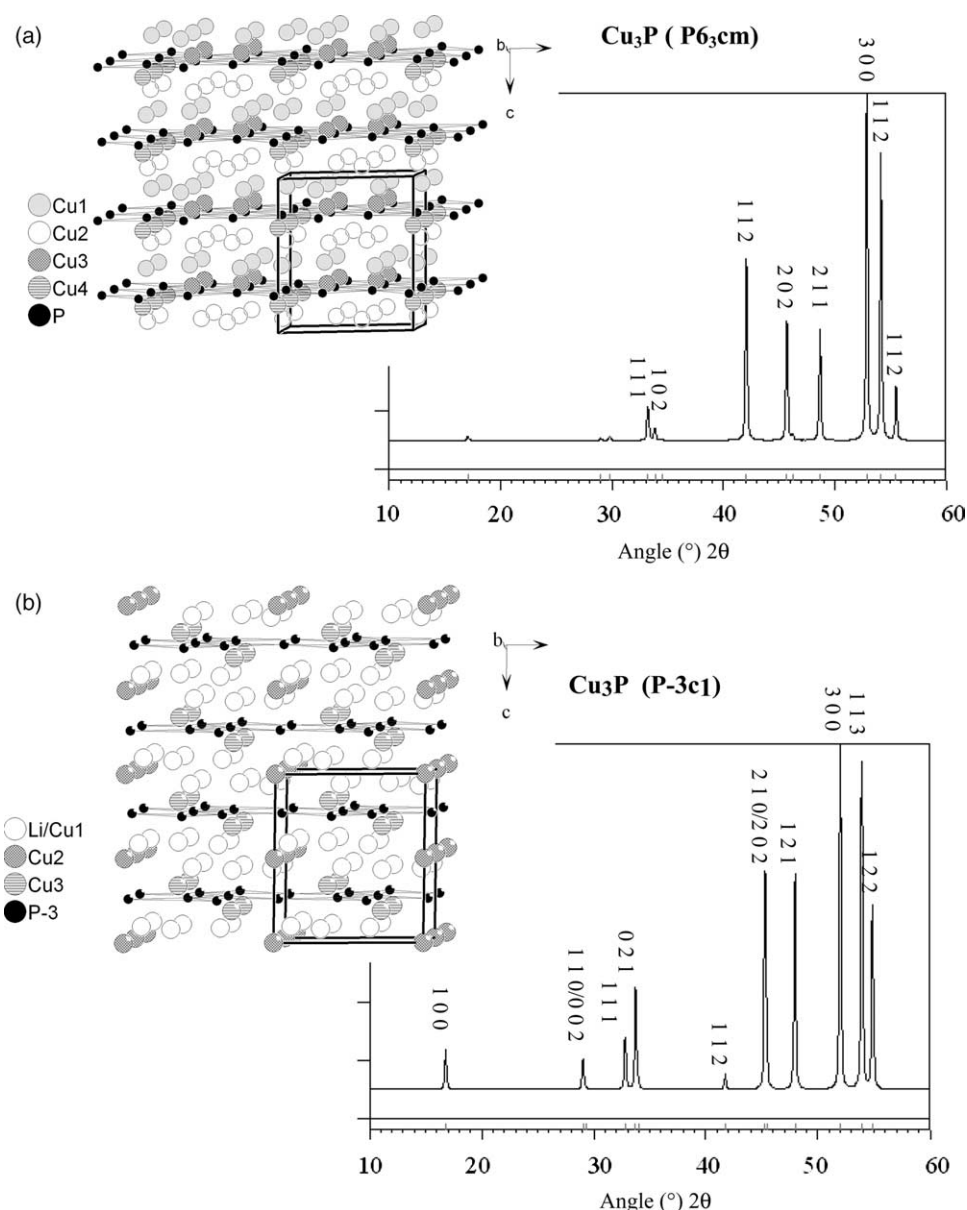


Fig. 5. Crystal structure represented in a $2 \times 2 \times 2$ unit cell of the Cu_3P ($P6_3cm$) (a) (PCPDF-71-2261) and of Cu_3P ($P-3c1$) (PCPDF-72-1330) in (b) and their powder XRD patterns, respectively.

yielding $\text{Li}_x\text{Cu}_3\text{P}$. Instead, it confirms that a Li/Cu substitution is most likely to occur as soon as discharge begins. The fact that no copper extrusion was identified from the XRD patterns in this part of the discharge can be easily explained by the poor diffusing power of finely divided Cu° particles, in small amount. Various Li/Cu substitutions have thus been calculated for $x=1/3$. Among the different copper atoms, Cu(1) and Cu(2) are the preferred atoms to be substituted as they are less linked to the phosphorus planes than Cu(3) and Cu(4). This is confirmed by an overlap population analysis performed on the different Cu(*i*)–P bonds (*i*=1, 2, 3, 4) [13]. Three different lithium distributions were thus investigated, in which Cu(1) and/or Cu(2) are substituted. The results are listed in Table 1, in which the notation 1+2, 1+1 and 2+2 stand for the different substitutions of two copper atoms among the 18 atoms present in the Cu_{18}P_6 unit cell. The results clearly show that several $\text{Li}_{0.33}\text{Cu}_{2.66}\text{P}$ phases are thermodynamically stable and energetically close to each other (within 10^{-2} eV). They correspond to a slightly greater unit cell parameter *a* than for the Cu_3P starting form. It is worth noting however, that the symmetry lowering induced by the Li/Cu substitution leads to a transition from the $P6_3cm$ to the $P-3c1$ space group. The latter actually corresponds to another reported form of Cu_3P ($a=7.070$ Å, $c=7.135$ Å; PCPDF 72-1330). In this symmetry, the two Cu(1) and Cu(2) copper atoms do not lie any longer on two different crystallographic positions (Fig. 5a) but on one 12-fold position (Fig. 5b), considering a statistical distribution of both Li and Cu on this twelve-fold position. The diffraction pattern of the Cu_3P structure described in the $P-3c1$ symmetry (Fig. 5b) shows a greater intensity for the (2 0 2) peak observed at 45.6° in 2θ than in the $P6_3cm$ symmetry (Fig. 5a). This may likely explain the increase of the electrode diffraction power seen in the in situ XRD patterns of Fig. 4a and d, around $x=0.2$ – 0.3 . This hypothesis is corroborated by the evolution of the other peaks. These results tend to confirm that $\text{Li}_x\text{Cu}_{3-x}\text{P}$ phases (up to $x=1$) can be easily stabilized by lithium electrochemical insertion, without drastic changes in the XRD patterns. Above this critical composition, a structural phase transition is observed to form the Li_2CuP phase. For this latter structure, perfect agreement is obtained between theory and experiments, as depicted by the unit cell parameters reported in Table 1.

At the end of discharge, no Li_3P diffraction peaks could be observed in the XRD patterns, although this phase exhibits a hexagonal structure, confirmed by structural relaxations (Table 1) [13]. However, the content of Cu° produced during (4) suggests that the last reaction corresponds to: (c) $\text{Li}_2\text{CuP} + \text{Li} \rightarrow \text{Li}_3\text{P} + \text{Cu}^\circ$.

During the charge, our results have revealed one extra process compared to the discharge. The diffraction peak areas plotted in Fig. 4d clearly show a large gap of about one lithium between the disappearance of Li_2CuP and the growth of Cu_3P . This gap has not been clearly associated with an extra phase, although the Cu° XRD peak decreases. Owing to the number of lithium

exchanged during this event, it seems clear that an intermediate amorphous LiCu_2P phase is formed. This hypothesis is strongly supported by the results reported previously for Cu_3P samples obtained from solvothermal synthesis routes [8]. In this work, an intermediate LiCu_2P was formed upon charge, yielding one more process in oxidation compared to the reduction. The reasons why this phase was not identified in discharge are still unknown. Theoretical calculations are in progress to address this question. Be that as it may, we can propose that the additional electrochemical reaction involved in charge for Cu_3P corresponds to: $\text{Li}_2\text{CuP} + \text{Cu}^\circ \rightarrow \text{LiCu}_2\text{P} + \text{Li}$.

5. Conclusion

The electrochemical reactivity of Cu_3P –HT towards lithium leads to close gravimetric capacity (377 vs. 372 mAh/g) and greater volumetric capacity (4732 vs. 830 mAh/cm³) than the theoretical capacity of graphite due to a much greater density for Cu_3P . Moreover, the extra capacity observed in Cu_3P compared to theoretical values, is explained in terms of irreversible lithium insertion in the CuP_2 XRD-amorphous impurity and SEI reactions. To get deeper in the identification of a SEI formation at the electrode/electrolyte interface, impedance spectroscopy measurements would be very helpful as the observation of second semi-circle, at high-frequencies, in the Nyquist plot.

The good volumetric capacity of Cu_3P could make it a good candidate for anode materials, a fortiori if its rather good capacity retention is further confirmed upon hundreds of cycles.

Acknowledgements

Authors thank the SAFT company for its financial support, M. Morcrette for in situ XRD measurements and F. Favier and M.P. Bichat for helpful discussion.

References

- [1] M.-P. Bichat, F. Gillot, L. Monconduit, F. Favier, M. Morcrette, F. Lemoigno, M.-L. Doublet, Chem. Mater. 16 (2004) 1002.
- [2] F. Gillot, M.-P. Bichat, F. Favier, M. Morcrette, M.-L. Doublet, L. Monconduit, Electrochim. Acta 47 (2004) 3137.
- [3] D.C.S. Souza, V. Pralong, A.J. Jacobson, L.F. Nazar, Science 296 (2002) 2012.
- [4] K. Wang, J. Yang, J. Xie, B. Wang, Z. Wen, Electrochem. Commun. 5 (2003) 480–483.
- [5] H. Pfeiffer, F. Tancret, M.-P. Bichat, L. Monconduit, F. Favier, T. Brousse, Electrochem. Commun. 6 (2004) 263.
- [6] O. Crosnier, C. Mounsey, P. Subramanya Herle, N. Taylor, L.F. Nazar, Chem. Mater. 15 (2003) 4890.
- [7] M.P. Bichat, T. Politova, H. Pfeiffer, F. Tancret, L. Monconduit, J.-L. Pascal, T. Brousse, F. Favier, Power Sources 136 (2004) 80.
- [8] M.-P. Bichat, T. Politova, J.-L. Pascal, F. Favier, L. Monconduit, J. Electrochem. Soc. 151 (2004) A2074–A2081.
- [9] G. Kresse, J. Hafner, Phys. Rev. B 47 (1993) 558.
- [10] G. Kresse, D. Joubert, Phys. Rev. B 59 (1999) 1758.
- [11] D. Vanderbilt, Phys. Rev. B 41 (1990) 7892.
- [12] O. Olofson, Acta Chem. Scand. 26 (1972) 2777.
- [13] M.L. Doublet, L. Monconduit, unpublished results.